S1 Supplementary Information (SI): Calmodulin/Calcineurin Interaction Beyond the Calmodulin-binding Region Contributes to Calcineurin Activation

Bin Sun[1], Darin Vaughan[1], Svetlana Tikunova[3],
Trevor P. Creamer[2], Jonathan P. Davis[3] and PM Kekenes-Huskey*[4,5]
[1] Department of Chemistry, University of Kentucky, [2] Department of Molecular & Cellular Biochemistry, University of Kentucky, [3] Department of Physiology and Cell Biology, Ohio State University, [4] Department of Chemical and Materials Engineering, University of Kentucky, Lexington, KY, USA 40506
[5 5] Department of Cell and Molecular Physiology, Loyola University Chicago, Maywood, IL, USA 60153
* Corresponding authors. E-mail address: pkekeneshuskey@luc.edu (P. Kekenes-Huskey)

S1.1 Methods

The initial structure corresponding to CaN distal helix to AID region (residues 459 to 490) was built from sequence via tleap. The initial structure was subjected to minimization and MD simulation in vacuum according to the procedure described Sect. 3.3. The optimized structure was then appended to the C-terminus of distal helix region from the representative structure of site D simulations via tleap. The representative structures of the first two most populated clusters from site D simulations were selected, making the simulation duplicate. The sytem was then solvated in TIP3P waterbox with 0.15 M KCl ions added. The simulation details are same as previous section in which the tleap built structure was first relaxed while rest part being fixed during the heating and equilibrium stage. After reaching equilibrium, about 0.7 μs production simulation was performed from each replica of the duplicate. The simulations were repeated for the CaN A454E mutant. The total number of MD cases considered in this study is listed in Table S3.

S1.2 Tables

Table S1: Residues at each tentative binding site on collapsed CaM used in ZDOCK to predict distal helix interaction at each site

Tentative Site	Residues
Site A	R86, F89, V142, Y138
Site B	R106, I125, D118, D122
Site C	I9, F12, L69, F65
Site D	K30 ,T34, R37, Q49

Table S2: ZDOCK docking scores of distal helix and DH_{A454E} at each site. During each docking, a culling process was applied on the initially generated 2×10^3 poses to eliminate those having no contacts with residues we specified in Table S1. After culling, the docking scores of highest-scored poses (up to 10 poses) are given. In DH-site A and DH_{A454E}-site B cases, there was no remaining poses left after culling, we instead output the first 10 poses' scores from the initially-generated 2×10^3 poses.

	site A		site B		site C		site D	
	DH	DH_{A454E}	DH	DH_{A454E}	DH	DH_{A454E}	DH	DH_{A454E}
pose 1	840.19	618.11	412.93	642.15	687.64	506.11	445.27	642.15
pose 2	786.35	617.84	378.87	629.03	668.06	505.23	414.33	629.00
pose 3	780.74	609.35		618.11	582.64	496.39	386.93	618.11
pose 4	726.30	608.15		617.84	572.20	482.48		617.84
pose 5	711.46	578.58		609.35	567.99	471.27		609.35
pose 6	705.07	564.20		608.15	564.11	470.38		608.15
pose 7	699.21	559.22		578.58	558.02	467.40		578.58
pose 8	681.33	550.57		567.75	550.77	465.25		567.75
pose 9	678.08	543.51		567.45	512.28	459.97		567.45
pose 10	670.06	537.14		564.20	505.47	457.62		564.20

Table S3: MD simulation cases.

Cases	Starting structure	Simulation length (ns)
CaN DH fragment	tleap built from sequence	100 ns REMD
CaN DH_{A454E} fragment	tleap built from sequence	100 ns REMD
site A	PDB 4q5u + ZDOCK-predicted	1 μs
site B	PDB 4q5u + ZDOCK-predicted	1.26 μs
site C	PDB 4q5u + ZDOCK-predicted	1.42 μs
site D	PDB 4q5u + ZDOCK-predicted	1.38 μs
CaM K30E	representative simulated structure from site D	1.22 μs
CaM G40D	representative simulated structure from site D	1.22 μs
CaN A454E	representative simulated structure from site D	1.1 μs
site D with AID added	representative simulated structure from site D	duplicates with 0.68 μs each
CaN A454E with AID added	representative simulated structure from CaN A454E	duplicates with 0.7 μs each

S1.3 Figures

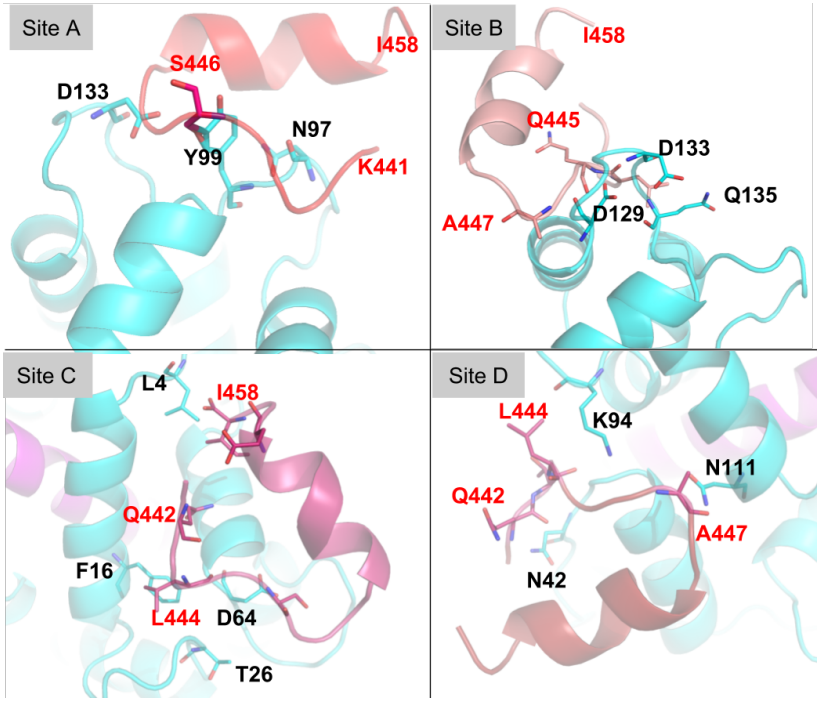

Figure S1: Highest-ranking CaM/distal helix interaction poses predicted by ZDOCK3.0.2 (32) webserver at each site. The color scheme is same as Fig. 2. Key residues at the interaction surface are shown in sticks with black labels for CaM residues and red labels for distal helix residues. Comparisons of the WT distal helix poses versus predictions for DH_{A454E} are shown in Fig. S2.

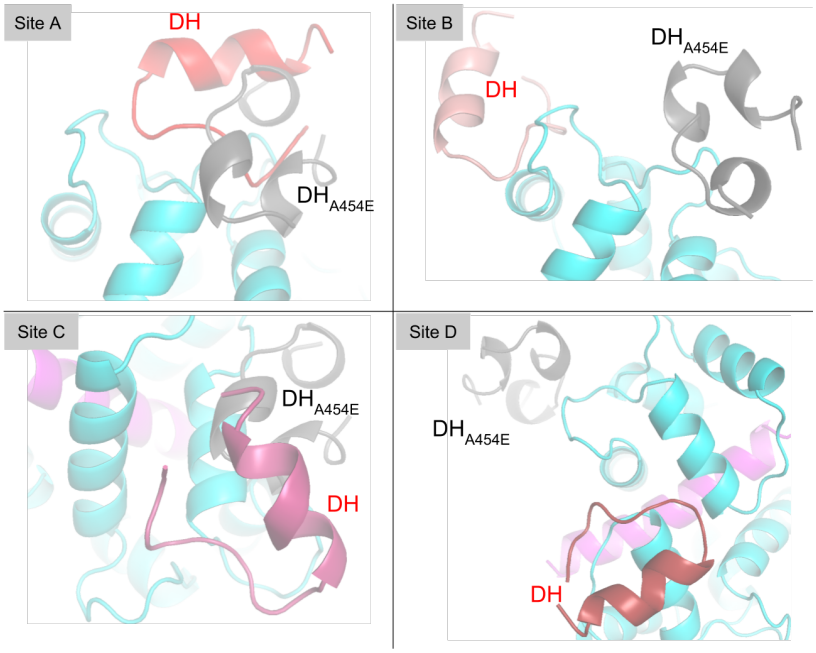

Figure S2: Comparison of Zdock predicted poses of DH and DH_{A454E} mutant at each site. The DH_{A454E} mutant is colored in gray. At site A and C, the poses of DH and mutant are close, while at site B and D, the DH_{A454E} mutant are predicted to be located near site A.

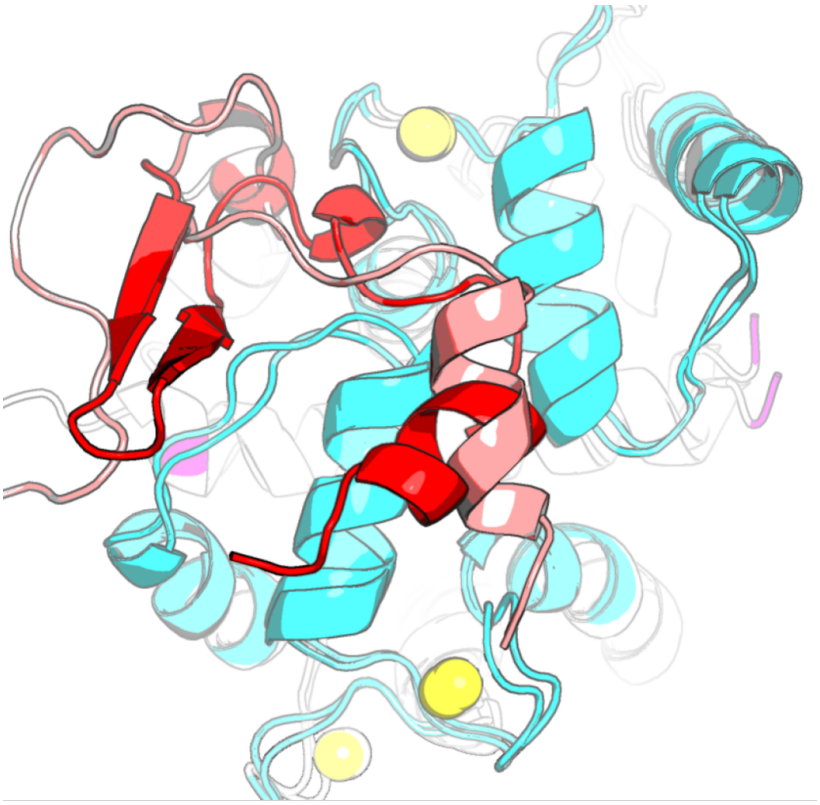

Figure S3: Overlap of MD simulated distal helix conformation starting at site B (colored in salmon) and site D (colored in red). During the simulations, distal helix starting at site B migrated to site D.

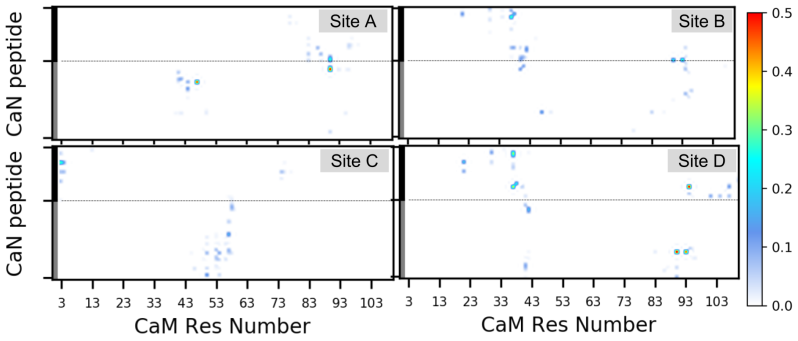

Figure S4: Percentage of simulated frames which have hydrogen bonds formed between CaN peptide (linker and distal helix) and CaM. The linker and distal helix are indicated by grey and black bars, respectively.

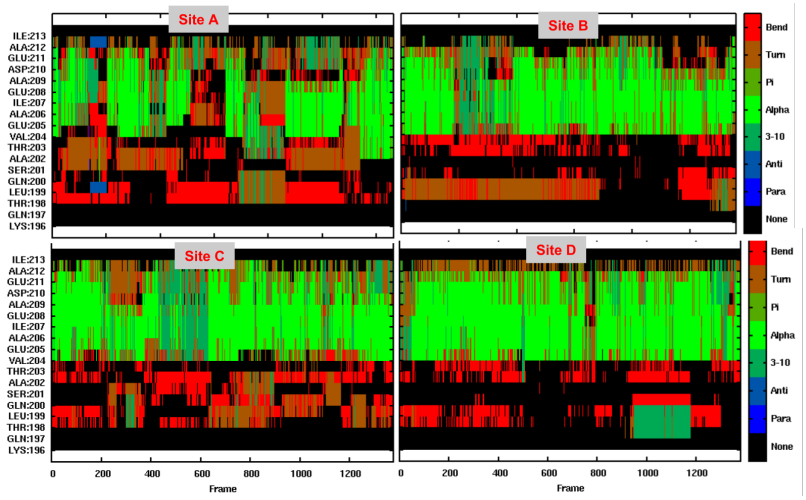

Figure S5: Secondary structure propensity of the distal helix during the MD simulations, as predicted via CPPTRAJ using the DSSP algorithm. The abundance of green indicates significant alpha helicity.

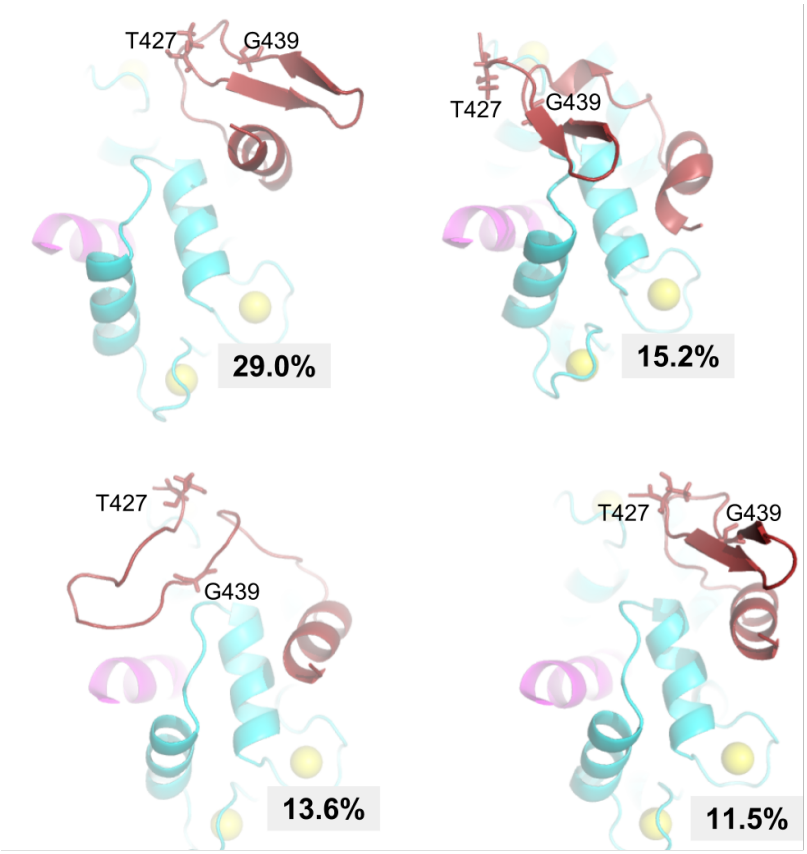

Figure S6: Illustration of β-sheet formed in T427-G439 region from site D simulations. The shown structures are representative structures of first four most populated clusters.

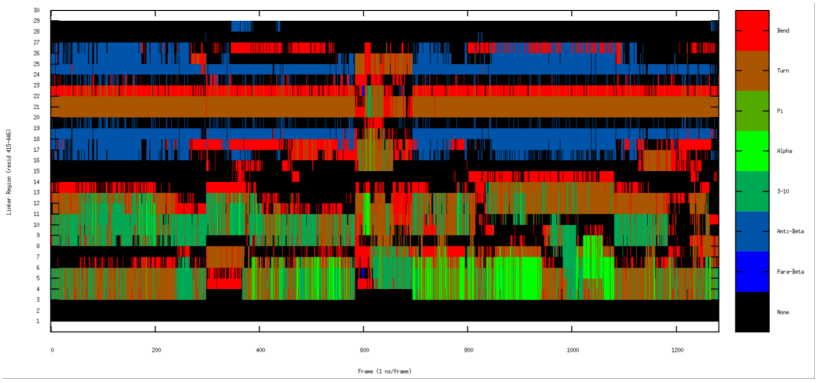

Figure S7: Secondary structure propensity of the linker at site D during the MD simulations, as predicted via CPPTRAJ using the DSSP algorithm. The blue region depicts the formation of β-sheet during most of the simulation time.

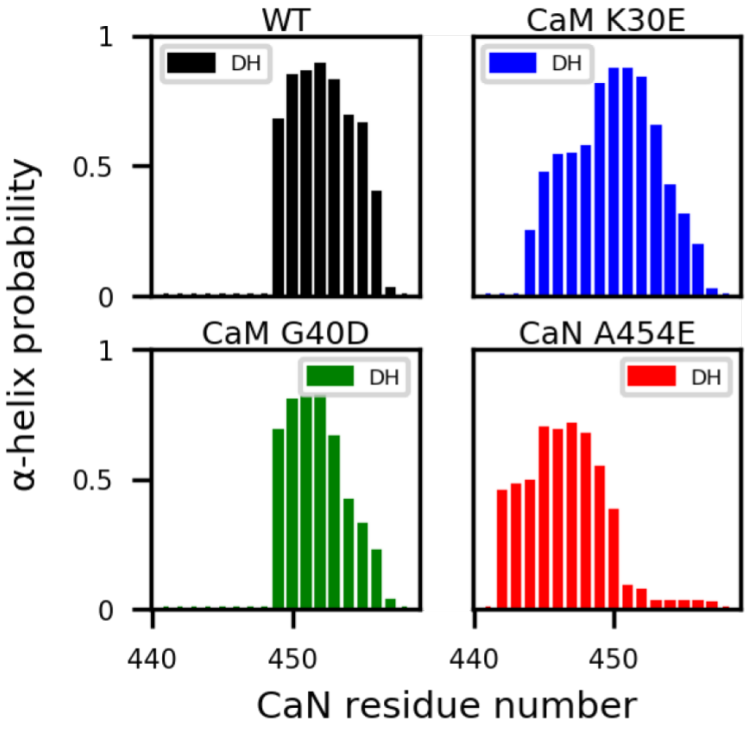

Figure S8: α-helix structural probability of each residue in distal helix region of WT, CaM K30E and G40D mutants and CaN A454E mutant calculated from MD simulations initiated at site D.

Table S4: Hydrogen bonds between distal helix and CaM in each case. Only hydrogen bonds sustained for >= 10% of the simulation duration are listed. The first residue is from distal helix and second residue is from CaM

Site A	Site B	Site C	Site D	CaM K30E	CaM G40D	CaN A454E
Q442-R90 0.17	K441-G40 0.10	Q442 R90 0.17	Q442 S101 0.10	Q445 S38 0.10	S446 T34 0.14	V459 K94 0.18
K441-R90 0.27	A457 R37 0.10	E453 L4 0.13	E450 K21 0.10	Q445 K21 0.10	S446 N111 0.16	A451 K94 0.28
	E445 N42 0.11	E453 Q3 0.28	E456 K30 0.11	A454 K115 0.10	E453 K30 0.19	
	L444 N42 0.12		Q445 H107 0.12	D455 K115 0.15	K441 N42 0.21	
	E456 K21 0.13		E453 K21 0.19	Q442 R37 0.19	D455 R37 0.22	
	E456 S38 0.17		S446 S38 0.23	L444 S38 0.29	Q442 N42 0.24	
	K441 R90 0.23		D455 R37 0.23	T448 T110 9.35		
	K441 D93 0.28		E456 R37 0.32			
	D455 R37 0.30		Q445 R37 0.37			
			Q445 K94 0.55			

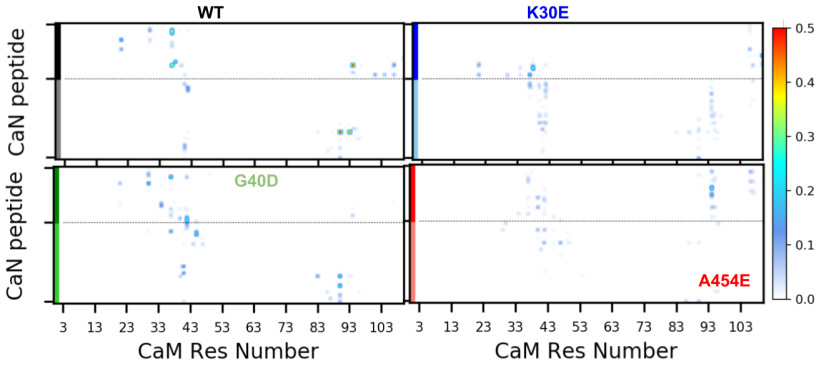

Figure S9: Percentage of simulated frame which have hydrogen bonds formed between the linker/distal helix and CaM for WT and variants at site D.

S1.4 Results

We calculated the backbone hydrogen bonds formed within the linker and distal helix region as an indicator of solvent-protection and compared this against experimental HXMS data. As shown in Fig. S10, WT site D has 16 hydrogen bonds with 2 dominant hydrogen bonds (red arrow) formed within the β-sheet region (Fig. S6). Also in the distal helix region, two long-lived hydrogen bonds (>40% simulation time) were found. Compared with other sites/mutants, backbone hydrogens at site D would be most protected from HXMS due to the larger number of hydrogen bonds and relatively longer duration. Although A454E has the largest number of hydrogen bonds, most are short-lived and the residue pairs that form hydrogen bonds are well-seperated in sequence, indicating that these hydrogen bonds do not contribute to α-helix secondary structure. Our computational modeling suggests that the putative distal helix region contains significant α-helical character when bound to CaM site D, which qualitatively agree with reduced susceptibility to hydrogen/deuterium exchange. Nevertheless, compared to experimental HXMS data that show solvent-protected hydrogens through out the linker and distal helix region, our computational backbone hydrogen bonds data indicate a lesser degree of solvent-protection as the majority of hydrogen bonds are present in the N terminus of linker region and C-terminus of distal helix region in site D. This discrepancy could be explained by the different lengths of CaN constructs used in HXMS experiment versus our simulations. The construct in HXMS experiment contains the entire RD domain including AID and the C-terminus, while our simulations contain residues of A391 to I458 of RD domain so as to have a computationally tractable system. To validate this assumption, we appended additional residues inclusive of the AID to the distal helix/CaM pose. The data in Fig. S12 demonstrate that appended residues enhanced the number and duration of backbone hydrogen bonds present in the linker and distal helix region. Additionally, several long-lived hydrogen bonds between the distal helix and CaM site D were found to stabilize the bound configuration, which dampened the fluctuations of peptide position found at other identified sites (A-C) as reported by RMSF and energetic analyses (Fig. S4).

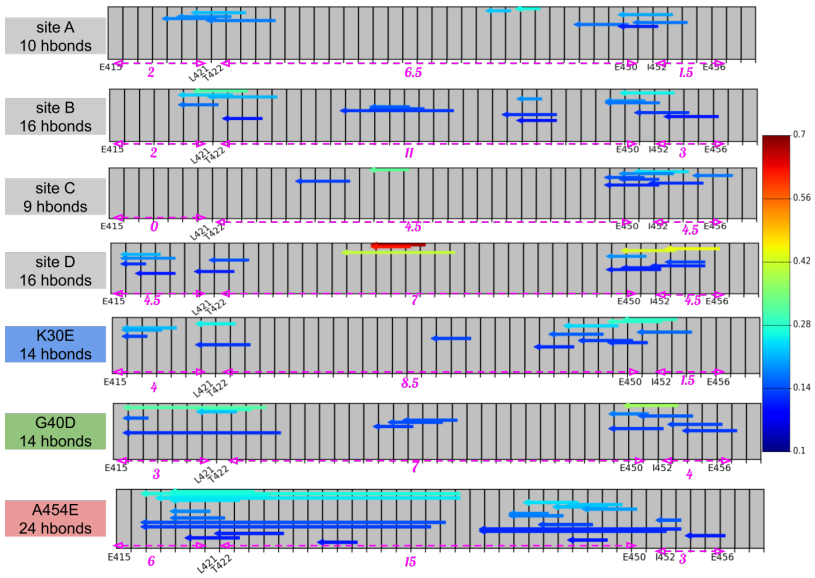

Figure S10: Backbone hydrogen bond analysis in the linker and distal helix region (E415 to I458) of CaN. Each arrow represents one hydrogen bond with color indicating percentage of simulated frames in which this hydrogen bond existed. Only hydrogen bonds existing >10% of simulation time are shown (we also show hydrogen bonds with >5% in Fig. S11). The whole region was divided into three subregions as indicated by the dashed magenta arrows below each subpanel. The subregion definition is consistent with the experimental HXMS data in Figure 8 in Rumi-Masante 2012 paper. The number under the magenta arrow depicts the number of hydrogen bonds in this subregion (one trans-subregion hydrogen bond contributes 0.5 to each subregion).

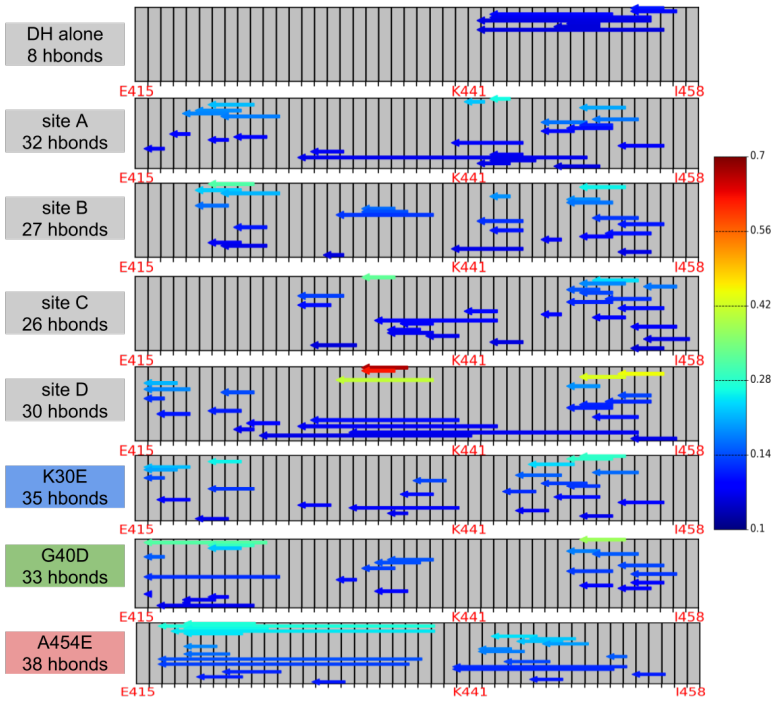

Figure S11: Backbone hydrogen bond analysis in the linker and distal helix region. Each arrow represents one hydrogen bond with color indicating percentage of simulated frames with this hydrogen bond existed. hydrogen bonds exist >5% of simulation time are shown.

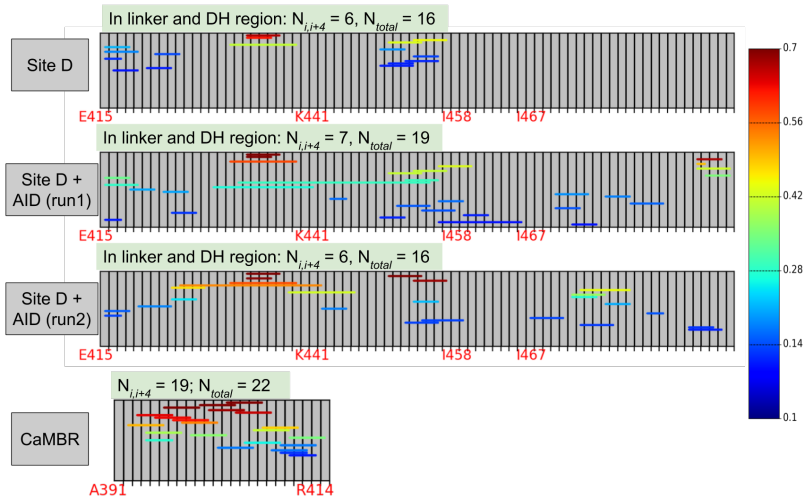

Figure S12: Comparison of backbone hydrogen bond in the linker and DH region between WT site D and WT site D with extra AID fragment added. The backbone hydrogen bond of CaMBR from WT site D is also show as reference. 1) In one of the two runs with AID added, the number of i,i+4 hydrogen bond (Ni,i+4) was increased by 1 due the presence of AID fragment, while the other run has value unchanged. 2) In both runs with AID added, the backbone hydrogen bonds become more stable as the duration of hydrogen bonds are generally enhanced. 3) The helicity of linker and DH region in site D (with/without AID) are much less stable than that of CaMBR, as indicated by smaller value of Ni,i+4, 6/7 vs. 19